



MATERIALS SCIENCE

Determination of the preferred epitaxy for III-nitride semiconductors on wet-transferred graphene

Fang Liu^{1†}, Tao Wang^{1,2†}, Xin Gao^{3,4†}, Huaiyuan Yang^{1†}, Zhihong Zhang^{5,6}, Yucheng Guo¹, Ye Yuan⁷, Zhen Huang¹, Jilin Tang^{3,4}, Bowen Sheng¹, Zhaoying Chen¹, Kaihui Liu^{1,6}, Bo Shen^{1,8}, Xin-Zheng Li^{1,6,8*}, Hailin Peng^{3,4,9*}, Xinqiang Wang^{1,8*}

Transferred graphene provides a promising III-nitride semiconductor epitaxial platform for fabricating multi-functional devices beyond the limitation of conventional substrates. Despite its tremendous fundamental and technological importance, it remains an open question on which kind of epitaxy is preferred for single-crystal III-nitrides. Popular answers to this include the remote epitaxy where the III-nitride/graphene interface is coupled by nonchemical bonds, and the quasi-van der Waals epitaxy (quasi-vdWe) where the interface is mainly coupled by covalent bonds. Here, we show the preferred one on wet-transferred graphene is quasi-vdWe. Using aluminum nitride (AlN), a strong polar III-nitride, as an example, we demonstrate that the remote interaction from the graphene/AlN template can inhibit out-of-plane lattice inversion other than in-plane lattice twist of the nuclei, resulting in a polycrystalline AlN film. In contrast, quasi-vdWe always leads to single-crystal film. By answering this long-standing controversy, this work could facilitate the development of III-nitride semiconductor devices on two-dimensional materials such as graphene.

INTRODUCTION

Wafer-scale single-crystal graphene can be mass-produced on several kinds of substrates, such as Cu(111) (1, 2), Cu-Ni alloy (3), and Cu(111)/Al₂O₃(0001) (4). The graphene can then be transferred to a target substrate surface (5–7), providing an attractive platform for fabricating III-nitride semiconductor devices. On such a platform, graphene can be used to alter the epitaxial relationship between the III-nitride semiconductor and the substrate, leading to single-crystal films on arbitrary substrates such as single-crystal Al₂O₃ (8, 9) and polycrystalline diamond (10). In addition, graphene enables intact interfacial separation of the film from the substrate, providing a simple method for developing flexible light-emitting devices (11, 12) via hetero-integration on epitaxy-incompatible functional templates. It is well known that high-quality single-crystal III-nitride films are required for the fabrication of high-performance devices (13, 14). To realize such III-nitride films on graphene, three different methods have been studied in recent years, namely, van der Waals epitaxy (vdWe) (15, 16), remote epitaxy (17, 18), and quasi-vdWe (8, 19). VdWe

is a process in which an upper film and substrate are combined by van der Waals forces, which is different from traditional epitaxy, where interfacial chemical bonding forms between the film and substrate (20, 21). However, the bond strength of van der Waals forces is normally one to two orders of magnitude lower than that of chemical bonds (22, 23). Therefore, it is difficult to achieve highly oriented nucleation and growth of single-crystal III-nitride films on graphene through van der Waals forces. The reported crystallinity and crystal quality of III-nitride films grown on graphene by vdWe are not as good as expected (24). In the case of remote epitaxy, interfacial interactions (nonchemical bonds) form between polar crystals and a graphene layer, and these interactions are stronger than van der Waals forces, resulting in a regular atomic arrangement of polar films (17). The lattice orientation coherence between the polar film and the polar template/substrate can be maintained even in the presence of a subnanometer-thick graphene interlayer. As previously reported (25), the remote epitaxy of single-crystal GaN films appears to have been realized on polar templates such as GaN(0001)/Al₂O₃(0001). In contrast, quasi-vdWe introduces covalent bonds at the interface, and this process takes advantage of defects on the graphene surface that provide unsaturated dangling bonds as nucleation sites to initiate highly oriented nucleation (26–28). The aligned nucleation islands expand and coalesce to form a single-crystal III-nitride film. In this case, the epitaxial film is coupled to the graphene interlayer via a combination of covalent bonds and van der Waals forces. Interfacial covalent bonds determine the epitaxial relationship between the upper layer and graphene (19, 29, 30). It seems that both quasi-vdWe and remote epitaxy can be used to place single-crystal III-nitride films on graphene. However, it is still a debate that which type of epitaxy is preferred for this application.

To answer this issue, we studied the growth of aluminum nitride (AlN) on a wet-transferred ultraflat graphene/AlN template. Here, a graphene/AlN template is chosen as an example because AlN is more polar than other III-nitrides (25, 31) and thus can provide a

¹State Key Laboratory for Mesoscopic Physics and Frontiers Science Center for Nano-optoelectronics, School of Physics, Peking University, Beijing 100871, China. ²Electron Microscopy Laboratory, School of Physics, Peking University, Beijing 100871, China. ³Center for Nano-chemistry, Beijing Science and Engineering Center for Nanocarbons, Beijing National Laboratory for Molecular Sciences, College of Chemistry and Molecular Engineering, Peking University, Beijing 100871, China. ⁴Academy for Advanced Interdisciplinary Studies, Peking University, Beijing 100871, China. ⁵Beijing Advanced Innovation Center for Materials Genome Engineering, Beijing Key Laboratory for Magneto-Photoelectrical Composite and Interface Science, Institute for Multidisciplinary Innovation, University of Science and Technology Beijing, Beijing 100083, China. ⁶Interdisciplinary Institute of Light-Element Quantum Materials, Research Center for Light-Element Advanced Materials, Peking University, Beijing 100871, China. ⁷Songshan Lake Materials Laboratory, Dongguan, Guangdong 523808, China. ⁸Peking University Yangtze Delta Institute of Optoelectronics, Nantong, Jiangsu 226010, China. ⁹Beijing Graphene Institute, Beijing 100095, China.

*Corresponding author. Email: wangshi@pku.edu.cn (X.W.); hlpeng@pku.edu.cn (H.P.); xzli@pku.edu.cn (X.-Z.L.)

†These authors contributed equally to this work.

stronger interfacial interaction for III-nitride remote epitaxy. In this case, it is found that the remote interaction from the graphene/AlN template can trigger nucleation and form AlN grains with the same lattice polarity as the underlying AlN template. However, remote epitaxy fails to suppress the in-plane twists of grains, leading to twisted III-nitride grains and polycrystalline films. On the other hand, quasi-vdWe leads to a single-crystal III-nitride film on transferred graphene with an epitaxial relationship of $\text{AlN}(10\bar{1}0)\|\text{graphene}(10\bar{1}0)$ and $\text{AlN}(11\bar{2}0)\|\text{graphene}(11\bar{2}0)$. This is attributed to that interfacial covalent bonds facilitate the maintenance of the epitaxial registry of the upper III-nitride layer and graphene. This work indicates that quasi-vdWe is the preferred method for the growth of single-crystal III-nitride films on wet-transferred two-dimensional materials such as graphene.

RESULTS

Theoretical model of III-nitride remote epitaxy

Wurtzite III-nitrides are non-centrosymmetric along the c axis, and they are two kinds of atomic arrangements along the $\langle 0001 \rangle$ direction that result in metal and nitrogen (N) lattice polarity. To study the remote epitaxy of AlN, eight atomic configurations/supercells were constructed (Fig. 1A and fig. S1). In configurations I and V, epitaxial AlN has the same atomic arrangement as the underlying AlN bulk. Keeping the spatial positions of the one-monolayer (ML) graphene and the AlN bulk unchanged, we performed the following operations on the epitaxial AlN in configurations I and V in sequence to obtain the other six configurations: an in-plane inversion (II and VI), an out-of-plane inversion (III and VII), and another in-plane inversion (IV and VIII). Please see Materials and Methods and Supplementary Materials (S1) for more details. To explore the effect of remote interaction on the atomic arrangement of the upper AlN, we then calculated the binding energies of the entire epitaxial AlN in eight configurations (Fig. 1B). It is shown that the binding energies of the epitaxial AlN in configurations I, II, V, and VI are considerably larger than those in configurations III, IV, VII, and VIII. The epitaxial AlN and AlN bulks in configurations I and II have Al lattice polarity, and the epitaxial AlN and AlN bulks in configurations V and VI have N lattice polarity, suggesting that the remote interaction tends to induce the growth of AlN films with the same lattice polarity as the bottom AlN template. That is, out-of-plane lattice inversion of remote epitaxial AlN is prohibited. Then, the contributions of van der Waals forces from graphene and remote atomic interactions in the form of nonchemical bonds from AlN bulk were estimated. The binding energies of epitaxial AlN on one-ML graphene/AlN bulk in configurations I, II, V, and VI (above -2 eV) are ~ 2 times larger than those driven only by remote atomic interactions (about -0.9 eV) and ~ 20 times larger than those driven only by van der Waals forces (about -0.1 eV), as shown in Fig. 1 (B and C). This demonstrates that the combination of graphene and AlN bulk provides a stronger driving force in the form of nonchemical bonds for AlN epitaxy than pure graphene or AlN bulk. This is because the electronic wave function of graphene is redistributed under the electrostatic field from the AlN bulk (32–34) when one-ML graphene is coupled to the AlN template. It is also found that the binding energies of epitaxial AlN (Fig. 1, B and C) in configurations I and II and in configurations V and VI are almost the same. This indicates that van der Waals

forces and remote atomic interactions are insensitive to the in-plane lattice inversion of epitaxial AlN, leading to their coupling being insensitive to it as well. Switching the epilayer and the bottom bulk from AlN to GaN (fig. S2), or one-ML graphene to one-ML h-BN (fig. S3), did not affect the tendency of the epilayer and the bulk layer to have the same lattice polarity. This is because the III-nitride represented by GaN and AlN is a polar material with a nonzero net electric dipole moment along the $[0001]$ direction. The dipole of the metal polar III-nitride points along the opposite direction with the dipole of the N-polar III-nitride. The interaction between the dipoles in the two III-nitride layers is strongest when they are orientated along the same direction (25, 35).

Next, the effect of graphene interlayer thickness on the remote epitaxy of AlN was explored. As shown in Fig. 1D, the binding energy of epitaxial AlN is the largest when one-ML graphene is used. As the number of graphene layers increases from one to three MLs, the binding energy decreases, showing that the remote interaction becomes weak. Notably, the binding energies of epitaxial AlN in configurations I, II, V, and VI are consistently larger than those in configurations III, IV, VII, and VIII, indicating that such remote interaction can still induce the growth of AlN grains with the same lattice polarity as the AlN bulk. Note that the binding energy of epitaxial AlN in configurations I, II, VII, and VIII is larger when the graphene thickness is greater than three MLs, indicating that the epitaxial AlN tends to have Al lattice polarity regardless of the lattice polarity of the AlN bulk. This phenomenon is attributed to the fact that the graphene/AlN bulk interaction cannot constrain the epilayer's lattice polarity, and van der Waals forces from graphene became dominant (fig. S1B). In this case, the effect of the polar AlN bulk is masked, and the growth pathway of upper AlN changes from the remote epitaxy to vdWe. The critical thickness of graphene that allows remote epitaxy is three MLs. Although the graphene has in-plane rotation with respect to the AlN bulk, the binding energy of epitaxial AlN is slightly affected, and the critical thickness of the graphene is not changed (fig. S4).

Next, to explore the effect of remote interactions on the in-plane orientation of AlN grains, we simplified the epitaxial AlN on one-ML graphene/AlN bulk in configurations I, II, V, and VI (Fig. 1A) to AlN clusters (R-AlNs) and thus obtained configurations RI, RII, RV, and RVI (Fig. 1E). Other parameters and periodic boundary conditions remain unchanged. It is found that the R-AlN in these configurations has the largest binding energy when there is 30° in-plane rotation relative to the AlN bulk (Fig. 1, F and G). When the R-AlN is rotated by 60° in-plane relative to the underlying AlN bulk (in configurations RI and RVI) or not rotated (in configurations RII and RV), its binding energy is minimal. This indicates that the atomic arrangement of AlN nuclei tends to have an in-plane rotation angle of 30° with the bottom AlN bulk to establish stronger interfacial coupling. However, since the energy gap between the maximum and the minimum is very small, ~ 0.095 eV (in configurations RI and RII) and ~ 0.140 eV (in configurations RV and RVI), the actual atomic arrangement in the upper AlN and the bottom AlN template may not exhibit a perfect in-plane 30° rotation relative to one another. Here, the rotational energy barrier of the R-AlN is defined as the minimal energy required for 30° in-plane rotation, which is approximately 0.077 eV in configurations RI and RII (yellow region, Fig. 1F), and approximately 0.099 eV in configurations RV and RVI (yellow region, Fig. 1G). It is well known that the growth temperature of single-crystal III-nitrides in metal-organic

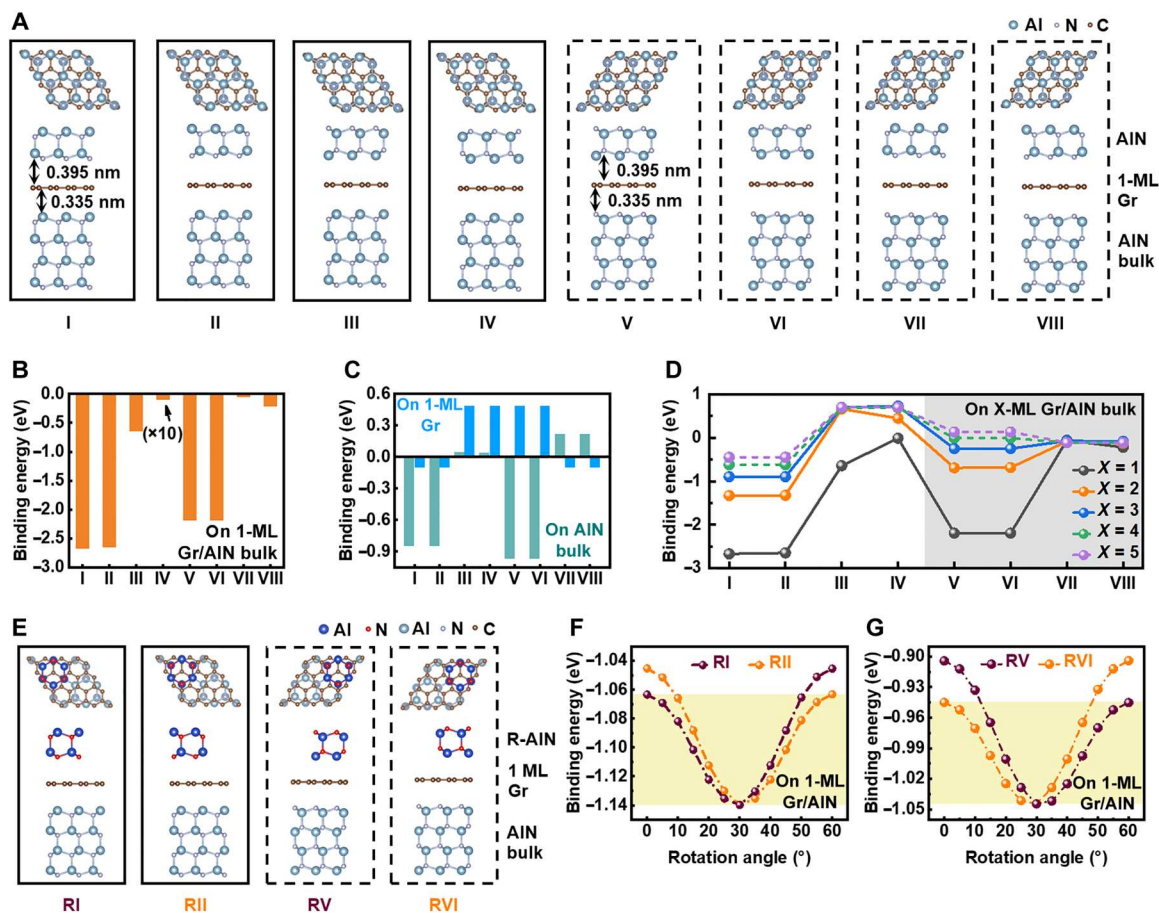


Fig. 1. Remote epitaxy model of AlN. (A) Density functional theory–modeled atomic structure of a remote epitaxial AlN layer on one-monolayer (ML) graphene (Gr)/AlN bulk. Top and side views are provided here. The AlN bulk in configurations I to IV has Al lattice polarity, while that in configurations V to VIII has N lattice polarity. The epitaxial AlN in configurations I, II, VII, and VIII has Al lattice polarity, while that in configurations III, IV, V, and VI has N lattice polarity. (B) Calculated binding energies of epitaxial AlN in configurations I to VIII. (C) Calculated binding energies of epitaxial AlN driven by either the remote atomic interaction from the AlN bulk (depicted in cyan) or the van der Waals force from the one-ML Gr (depicted in blue). (D) Binding energies of epitaxial AlN as a function of Gr interlayer thickness. The thickness of Gr interlayers is one to five MLs. (E) Atomic models of AlN nuclei (R-AlN) on one-ML Gr/AlN bulk. The R-AlN structure is in-plane rotated clockwise by 0° with respect to the underlying AlN bulk. (F and G) Calculation results of the rotational energy barrier of R-AlN with Al lattice polarity (F) or N lattice polarity (G) on a one-ML Gr/AlN bulk. Since AlN has sixfold symmetry, a clockwise rotation of R-AlN with respect to the bottom AlN bulk in the range of 0° to 60° is considered.

chemical vapor deposition (MOCVD) typically exceeds 1000°C (14, 36, 37). The corresponding thermal energy ($k_B T$, where k_B is the Boltzmann constant, and T is the growth temperature) of AlN nuclei (~ 0.110 eV) exceeds the calculated rotational energy barriers for R-AlN. Even if the growth temperature is decreased to 600°C , the corresponding thermal energy of the AlN nucleus still exceeds 0.070 eV. Such a small energy gap (Fig. 1, E to G) means that the in-plane rotation of nuclei is difficult to control spontaneously, i.e., the twist of the nuclei may be very large, which results in the formation of a polycrystalline III-nitride film composed of twisted grains. The epitaxial GaN/one-ML graphene/GaN bulk system (fig. S2) and epitaxial AlN/one-ML h-BN/AlN bulk system (fig. S3) show a similar trend to epitaxial AlN/one-ML graphene/AlN bulk system. In addition, to study the size effect of the remote interaction on the in-plane orientation of AlN nuclei, a big configuration RI is constructed (fig. S5). It was found that big AlN nuclei also tend to in-plane rotate with AlN bulk for greater binding energy. These results indicate that the spontaneous formation of highly oriented nuclei seems

to be difficult, and the remote epitaxy of single-crystal III-nitrides needs to break through certain technical barriers.

Remote epitaxy of AlN films

Considering that the surface wrinkles and point defects of the graphene layer are preferred nucleation sites for quasi-vdWe (27), we choose ultraflat single-crystal graphene MLs grown on Cu(111)/ $\text{Al}_2\text{O}_3(0001)$ as the interlayer for remote epitaxy. Compared with the one-ML graphene grown on Cu(111) foil, the ultraflat graphene ML after the wet transfer has a flatter surface (fig. S6). It should be acknowledged that even when the graphene material was optimized, a small number of breakages were still observed in one-ML graphene after the transfer, and structural imperfections such as wrinkles and bubbles were observed in two- to three-ML graphene. This is the common morphology of wet-transferred graphene (37, 38). Then, the MOCVD growth temperature of 500 nm thick AlN films on wet-transferred ultraflat graphene/AlN templates was kept at 1000°C to suppress the point defects which may

markedly increase when the graphene/AlN template is heated to a higher temperature in the MOCVD chamber (fig. S7).

In scanning transmission electron microscopy (STEM) and scanning electron microscopy (SEM) measurements (Fig. 2 and figs. S9 and S10), after excluding the obstruction of nonremote epitaxial AlN components, it is found that remote epitaxial AlN has a polycrystalline structure on wet-transferred one- to three-ML graphene, regardless of the lattice polarity of the upper layer and the AlN template. The remote epitaxial AlN (figs. S9 to S11) appears to consist of grains. The orientation relationship between the AlN grain and the AlN template is studied. It is found that when the AlN(0001)/Al₂O₃(0001) template is used, the atomic arrangement of the remote epitaxial AlN along the growth direction, i.e., [0001] direction, is the same as that of the AlN template layer, even when the thickness of the graphene layer is increased from one to three MLs (Fig. 2A). It means that out-of-plane lattice inversion of nucleus is prohibited, and the expansion of the nucleus into the grain results in Al lattice polarity. However, although the one-ML graphene/AlN template provides strong remote interactions for

remote epitaxy (Fig. 1D), the upper film has a polycrystalline structure consisting of misoriented grains (figs. S9 and S10). The deformed AlN grains do not have a fixed in-plane orientation relationship with the AlN(0001) template, making it difficult to obtain clear atomic-resolution images of the upper AlN grain and bottom AlN template layer simultaneously with high-angle annular dark-field STEM (HAADF-STEM). Next, the twist angles of the upper AlN relative to the AlN template are measured. In the interfacial region below four randomly selected grains, the in-plane twist angles of the upper AlN are 0.8° (Fig. 2B), 6.5° (Fig. 2C), 26.9° (Fig. 2D), and 0° (Fig. 2E) with respect to the bottom AlN template. The upper AlN (Fig. 2, B to D) has almost no out-of-plane tilt at the one-ML graphene-covered flat AlN template position. At the one-ML graphene-covered trenched AlN template position (Fig. 2E), the upper AlN has an out-of-plane tilt angle of 18.5° with respect to the AlN template. This tilt angle is close to the angle between graphene and the underlying AlN template along the *c* axis, and AlN has the same [0001]-axis direction as one-ML graphene (fig. S11D). Thus, AlN growth here is more likely to be controlled by one-ML

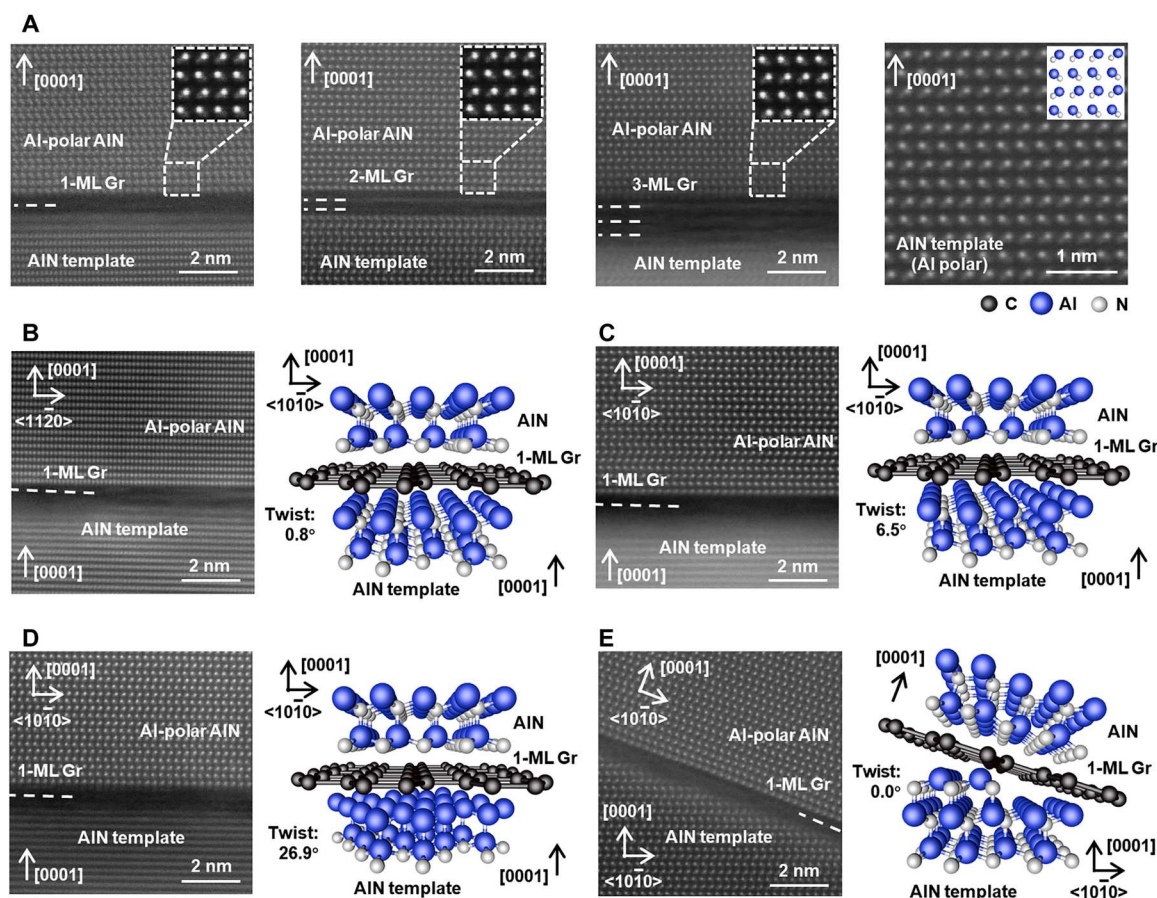


Fig. 2. STEM measurement results of remote epitaxial AlN with Al lattice polarity. (A) High-angle annular dark-field STEM (HAADF-STEM) images of remote epitaxial AlN on one- to three-ML Gr/AlN(0001) template. Both the upper and bottom AlN layers have Al lattice polarity, and the thicknesses of the Gr interlayers are one, two, and three MLs. The growth direction of the upper AlN is parallel to the [0001] axis of the AlN(0001) template. (B to E) HAADF-STEM images and corresponding atomic models of different remote epitaxial AlN/one-ML Gr/AlN interface regions. It is difficult to obtain clear atomic resolution images of two AlN layers simultaneously in HAADF-STEM images because the upper AlN and AlN templates have in-plane twist. By adjusting the lamella zone axis, a clear atomic resolution image of the upper AlN can be obtained. The twist angles of the AlN grain relative to the underlying AlN template are 0.8° (B), 6.5° (C), 26.9° (D), and 0° (E). In the flat template region, the upper AlN (B to D) and underlying AlN templates have the same lattice polarity, and the tilt angle is always less than 0.5°. In a small number of trenched template regions, the tilt angle of the AlN grain (E) is 18.5° relative to the underlying AlN template.

graphene than by a combination of one-ML graphene and AlN template. It should be pointed out that the spacing between graphene MLs in some interface areas may slightly deviate from the values in the atomic model (fig. S1A). This mainly comes from the imperfection of wet transfer. But even in the near-ideal interface region, the AlN grain still has in-plane rotation with respect to the bottom AlN template (fig. S11B). On the other hand, the surface fluctuation of graphene may cause the epitaxial AlN to have a small-angle tilt with respect to the AlN template. These results indicate that the remote interaction from the transferred graphene/AlN(0001) template is not strong enough to spontaneously constrain the random twist of grains at the planar template position or the tilt at a specific angle at the trenched template position, resulting in a polycrystalline film. This claim was further confirmed. It is found that remote epitaxial AlN on one- to two-ML graphene/AlN(0001) template can be stripped from the AlN template to the blue tape. Both the electron backscattered diffraction (EBSD) measurement before tape-assisted stripping and the x-ray diffraction (XRD) measurement after stripping (figs. S12 and S13) show that the film does have a *c*-axis orientation, but no in-plane preferred orientation.

To explore the effect of an N-polar AlN template on the remote epitaxial AlN, 500 nm thick AlN films grown on graphene/AlN(000 $\bar{1}$) templates are studied. As depicted in fig. S12 (B and C), the remote epitaxial AlN is also composed of grains. It is found that the remote epitaxial AlN (Fig. 3A) and GaN (Fig. 3B) grains near the graphene interlayer have the same lattice arrangement along the growth direction as the underlying AlN(000 $\bar{1}$) template, that is, both have N lattice polarity. This indicates that remote interactions from the graphene/AlN(000 $\bar{1}$) template can drive the nucleation of III-nitrides with N lattice polarity. As a special case, the lattice polarity of the AlN film with initial N lattice polarity may be inverted in the subsequent growth process. As we previously reported (19), the formation of a thin AlON transition layer leads to lattice polarity reversion in AlN grown by MOCVD. Hence, the remote epitaxial AlN grains invert to have Al lattice polarity (Fig. 3A), while the remote epitaxial GaN grains maintain their N lattice polarity (Fig. 3B). Subsequently, the in-plane orientation of AlN grains is evaluated. It is found that when the thickness of the graphene interlayer is one ML, the AlN grain exhibits twists of 0.1° (Fig. 3C), 4.8° (Fig. 3D), 16.6° (Fig. 3E), and 29.8° (Fig. 3F) relative to the bottom AlN template at four different interface regions. This suggests that the remote interaction provided by the graphene/N-polar AlN template also fails to constrain the in-plane orientation of AlN nuclei and grains. The above results show that the remote epitaxial AlN on wet-transferred graphene tends to have a polycrystalline structure consisting of twisted grains, which is independent of the lattice polarity of AlN (Figs. 2 and 3) and regardless of whether the graphene interlayer thickness is one, two, or three MLs (figs. S9 and S12). Thus, clear domain structures can be observed on the stripped AlN surface (fig. S13, C and F), i.e., the underside of the AlN near the graphene layer.

Quasi-vdWe of III-nitride films

Here, graphene interlayers with thicknesses of one, two, and three MLs were transferred to the surface of AlN(0001) templates. The graphene/AlN templates were irradiated by atomic N to form unsaturated C–N dangling bonds on the surface (8, 26, 28, 29). The dangling bonds serve as nucleation sites to initiate III-nitride growth.

The radiation parameters of graphene need to be finely regulated to ensure adequate graphene integrity (figs. S15 and S16, A and B). Then, 500 nm thick AlN films were grown by MOCVD at 1000°C with the same growth parameters as those of the remote epitaxy process. Figure 4A shows the EBSD measurement results of quasi-van der Waals epitaxial AlN films. The color distribution in the inverse pole figure (IPF) map is monochromatic, which indicates the single-crystal structure of the film. XRD measurements (fig. S16D) further confirm the good crystal quality of the film. This suggests that interfacial covalent bonds are beneficial for maintaining the epitaxial registry of upper AlN film and graphene as expected. Notably, quasi-van der Waals epitaxial AlN films on one- to three-ML graphene can be stripped. When the graphene thickness was one ML, the graphene ML was not perfect (39, 40) due to transfer damage and high-temperature damage, resulting in that the film cannot be fully stripped (fig. S15B). When the graphene thickness is larger than one ML, the AlN film can be almost completely separated from the substrate to the blue tape (fig. S15, C and D). This is because a thicker graphene layer has better structural integrity during MOCVD growth (fig. S9D). The fact that III-nitride films grew on one- to three-ML graphene/polycrystalline molybdenum (figs. S17 and S18) demonstrates that the III-nitride film forms an epitaxial relationship with graphene instead of the substrate, which is AlN(10 $\bar{1}$ 0)||graphene(10 $\bar{1}$ 0) and AlN(11 $\bar{2}$ 0)||graphene(11 $\bar{2}$ 0). It can be inferred that when graphene has in-plane rotation with respect to the AlN template, the epilayer follows graphene. Thicker graphene, such as three MLs, is beneficial for this as the key is to ensure the crystallinity and integrity of the graphene interlayer. This is because when thin graphene is used, such as one ML, upper III-nitrides may have a mixed growth mode consisting of quasi-vdWe and thru-hole epitaxy (fig. S15). The orientation relationship between the transferred graphene and the bottom AlN template must be well controlled (i.e., there is almost no in-plane rotation) to guarantee the crystal quality of the epitaxial film. As a result, those AlN grains obtained by quasi-vdWe and thru-hole epitaxy exhibit the same orientation, allowing rapid coalescence to form a continuous single-crystal film (Fig. 4A). When the graphene thickness increases to three MLs, the thru-hole epitaxy mode is almost completely shielded, and transferrable single-crystal III-nitride films can be obtained on arbitrary substrates by quasi-vdWe. To prove it, we transferred three three-ML graphene interlayers onto a 2-inch AlN(0001) template, and then grew 500 nm thick AlN films. The rotation angles of the graphene interlayer relative to the bottom AlN template are 8.4°, 75.3°, and 89.2°, respectively. The in-plane and out-of-plane orientations of those AlN films (Fig. 4B) were estimated using XRD 2 θ - ω and ϕ scans. The AlN (0002) Bragg diffraction peak can be identified at 36.0° for all films (Fig. 4C), confirming the fine out-of-plane orientation of the film. The in-plane ϕ scan of the upper AlN (10 $\bar{1}$ 2) plane shows sixfold symmetric diffraction from its single-crystal wurtzite structure (Fig. 4, C and D). As expected, the diffraction peaks of the (10 $\bar{1}$ 2) plane of epitaxial AlN on the three graphene regions are shifted by 8.4°, 15.3°, and 29.2° with respect to the diffraction peaks of (10 $\bar{1}$ 2) plane of the underlying AlN template. This indicates that similar to a twisted graphene bilayer (2), the designed growth of two single-crystal III-nitride layers with arbitrary twist angles can also be achieved.

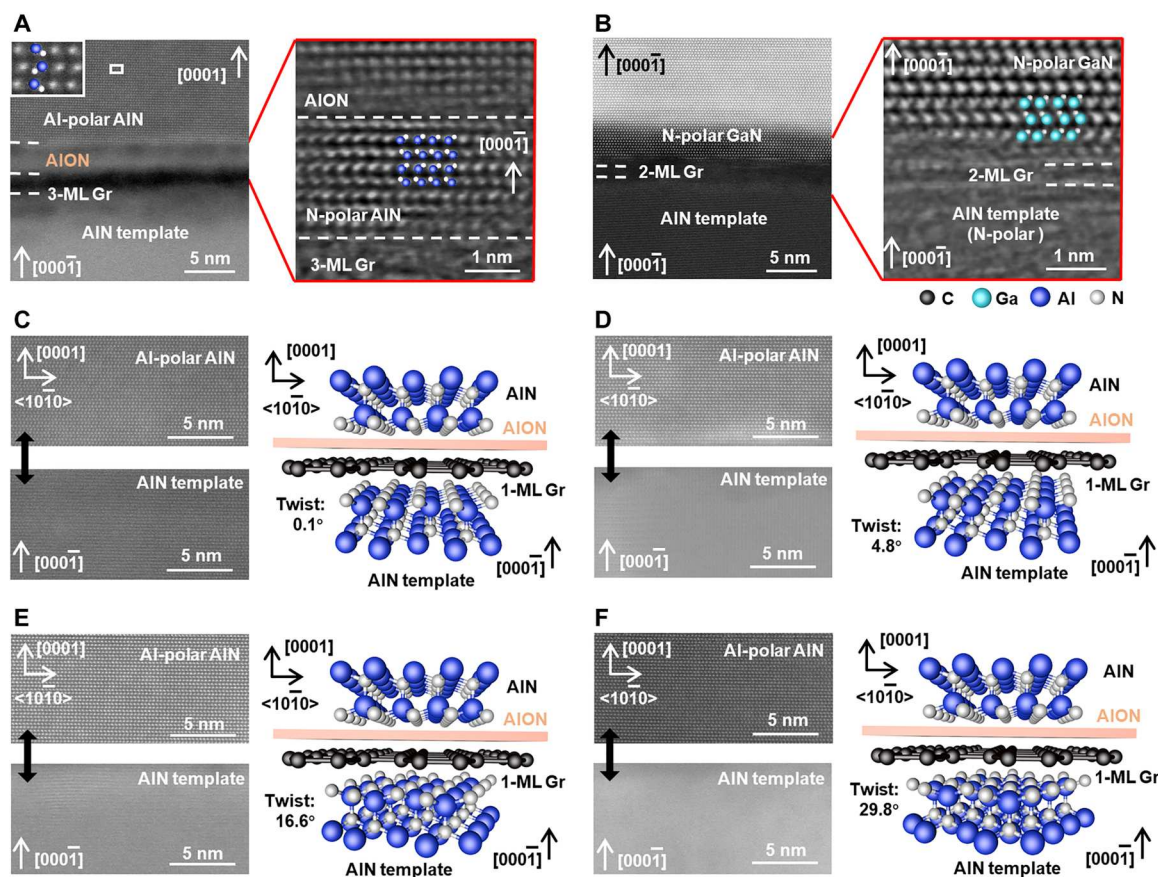


Fig. 3. STEM measurement results of remote epitaxial III-nitride films on N-polar AlN templates. (A) HAADF-STEM and integrated differential phase contrast (iDPC)-STEM images (red box) of remote epitaxial 500 nm thick AlN on the three-ML Gr/AlN(000 $\bar{1}$) template. The remote interaction drives the nucleation of N-polar AlN, but the formation of a thin AlON transition layer inverts the lattice polarity of the upper layer to Al lattice polarity (19). Graphene is simply labeled Gr. (B) HAADF-STEM and iDPC-STEM images (red box) of remote epitaxial 500 nm thick GaN on a two-ML Gr/AlN(000 $\bar{1}$) template. The GaN layer has N lattice polarity. The growth direction of the upper layer (A and B) is parallel to the [000 $\bar{1}$] axis of the N-polar AlN template. Electron beam irradiation damage during STEM measurement results in a certain degree of lattice damage near the Gr interlayer. (C to F) HAADF-STEM images and corresponding atomic models of the epitaxial AlN/one-ML Gr/AlN interface below four AlN grains. STEM measurement conditions are the same as those in Fig. 2 (B to E). The in-plane twist angles of the upper AlN relative to the bottom AlN template are 0.1° (C), 4.8° (D), 16.6° (E), and 29.8° (F). This suggests that the remote epitaxial AlN on the wet-transferred Gr/AlN (000 $\bar{1}$) template is also composed of randomly twisted grains.

DISCUSSION

So far, we propose a simple model for the remote epitaxy and quasi-vdWe of III-nitrides on wet-transferred graphene. The remote interaction from graphene/III-nitride templates can constrain the out-of-plane orientation of III-nitride nuclei but not the in-plane orientation, resulting in the formation of twisted grains (Fig. 5A). The misoriented grains expand and form a polycrystalline film, which is confirmed by planar STEM measurement (Fig. 5C). Considering that AlN is more polar than other III-nitrides and thus can provide the strongest known remote interaction to start remote epitaxy, it is reasonable to speculate that the remote interaction tends to drive twisted nucleation and then form a polycrystalline film for all III-nitrides on wet-transferred graphene/III-nitride templates. It should be pointed out that the structural integrity of the graphene interlayer has a substantial impact on the remote epitaxy of III-nitride because the III-nitride film will grow on the III-nitride template at graphene breakages (figs. S9 and S10). As growth proceeds, the nonremote epitaxial component with a faster growth rate will gradually dominate and cover the remote

epitaxial one, resulting in a single-crystal micrometer-thick film (fig. S14B). This process is no longer remote epitaxy but a special kind of epitaxial lateral overgrowth (ELOG) (41). As previously reported (17, 25, 42–45), remote epitaxy is a promising method for fabricating transferable III-nitride films and light-emitting devices. Remote epitaxy of single-crystal GaN(0001) films on graphene/GaN(0001) templates has been reported at a growth temperature of $\sim 700^\circ\text{C}$ by MBE (18, 24). This may be due to that the relatively low growth temperature limits the in-plane twist of the remote epitaxial grains to some extent, and MBE had a stronger ability to regulate the growth kinetics of III-nitride than MOCVD at low growth temperature. The structural damage caused by the N-plasma source in MBE (46) and the interference of the interfacial oxidation layer (47, 48) can be avoided by using MOCVD since the latter growth is performed at high temperatures as high as $\sim 1000^\circ\text{C}$ under hydrogen-containing ambient. In this case, the remote epitaxial grains on graphene show spontaneously twist and thus form a polycrystalline film (Figs. 2 and 5C). Our results are not inconsistent with previous results, as they both suggest

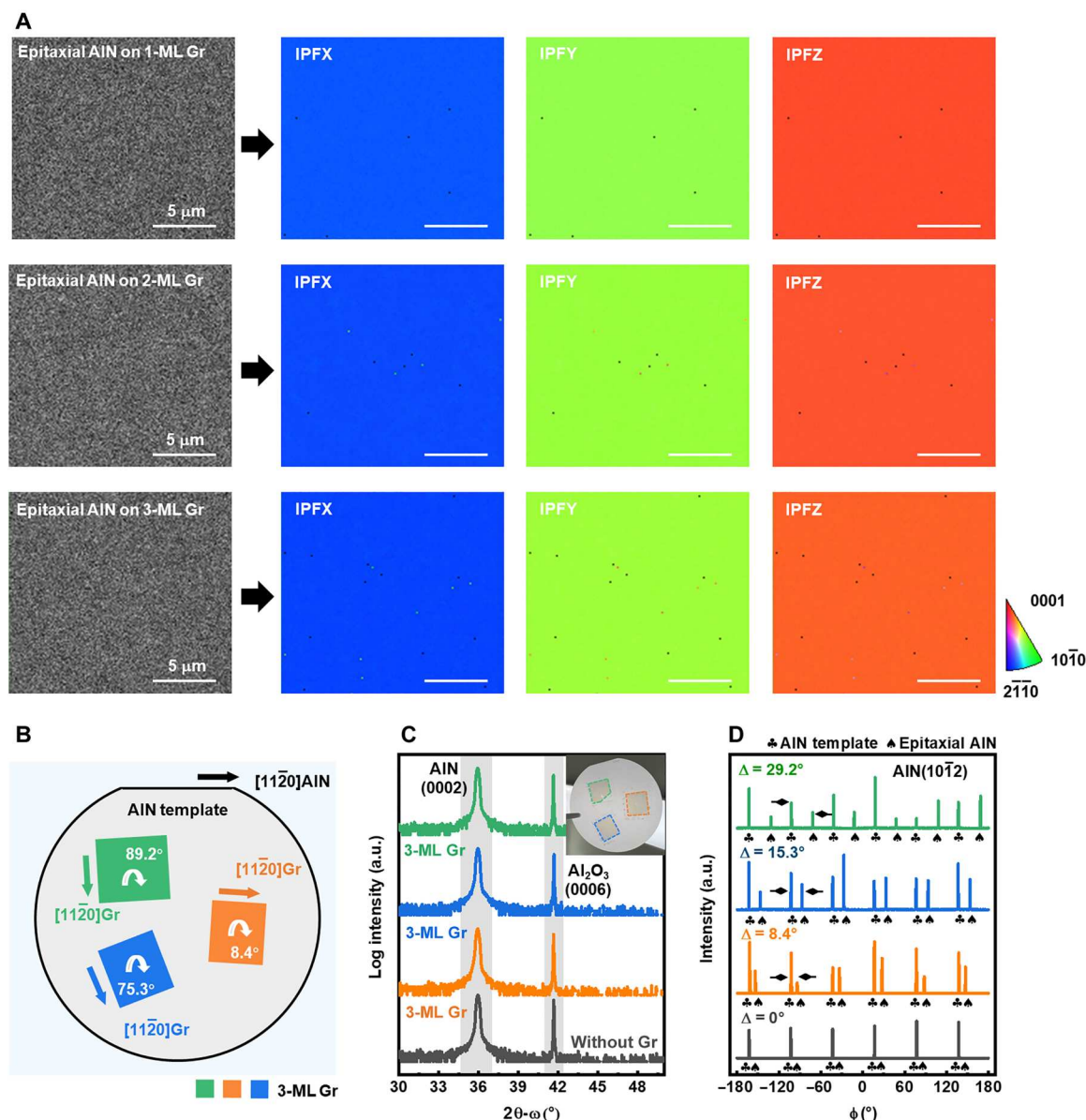


Fig. 4. Quasi-vdWe of single-crystal AlN films on irradiated graphene/AlN templates. (A) EBSD and in situ SEM images of 500 nm thick single-crystal AlN films grown on one- to three-ML Gr/AlN(0001) templates. Epitaxial AlN is coated with a conductive carbon layer with a thickness of 10 nm. Thus, the coarsening of SEM images is produced. The color distribution of the IPF images of the films is monochromatic, which is attributed to the films having a single-crystal structure. The IPFX, IPFY, and IPFZ images show the crystal orientation of the AlN film along the $[2\bar{1}\bar{1}0]$, $[10\bar{1}0]$, and $[0001]$ axes, respectively. These Gr layers have no in-plane rotation with respect to the underlying AlN template. All scale bars are 5 μm . (B) Schematic diagram of quasi-van der Waals epitaxial AlN films on three three-ML Gr regions on an AlN(0001) template. The Gr in the green, blue, and orange regions are in-plane rotated by 89.2°, 75.3°, and 8.4° with respect to the bottom AlN template, respectively. (C and D) XRD 2θ - ω scans (C) and ϕ scans (D) of 500 nm thick AlN grown on three-ML Gr/AlN(0001) templates. Epitaxial AlN films above the green, blue, and orange regions have in-plane rotation angles (Δ) of 29.2°, 15.3°, and 8.4° with respect to the underlying AlN template, respectively. This confirms that it is the wet-transferred Gr rather than the AlN template that determines the lattice orientation of the quasi-van der Waals epitaxial film. Graphene is simply labeled Gr. Atomic N irradiation times of one-ML, two-ML, and three-ML Gr are 1, 2, and 3 min, respectively. Please see Materials and Methods and fig. S15 for more details.

that the realization of single-crystal remote epitaxial III-nitride films requires excellent integrity and flatness of the graphene and optimizing the regulation of III-nitride growth kinetics. In addition, further study is needed on how to eliminate the interference of thru-hole epitaxy (49), pinhole-seeded lateral epitaxy (50), and quasi-vdWe (19) to achieve pure remote epitaxy of III-nitride by MBE or MOCVD.

On the other hand, quasi-van der Waals epitaxial III-nitride films can establish an epitaxial relationship with irradiated single-crystal graphene through interfacial covalent bonds (Fig. 5B), leading to nucleation islands with near-consistent orientation and forming a single-crystal film (Fig. 5D). The importance of interfacial chemical bonds in the formation of the epitaxial registry between the III-nitride film and graphene is emphasized. In this

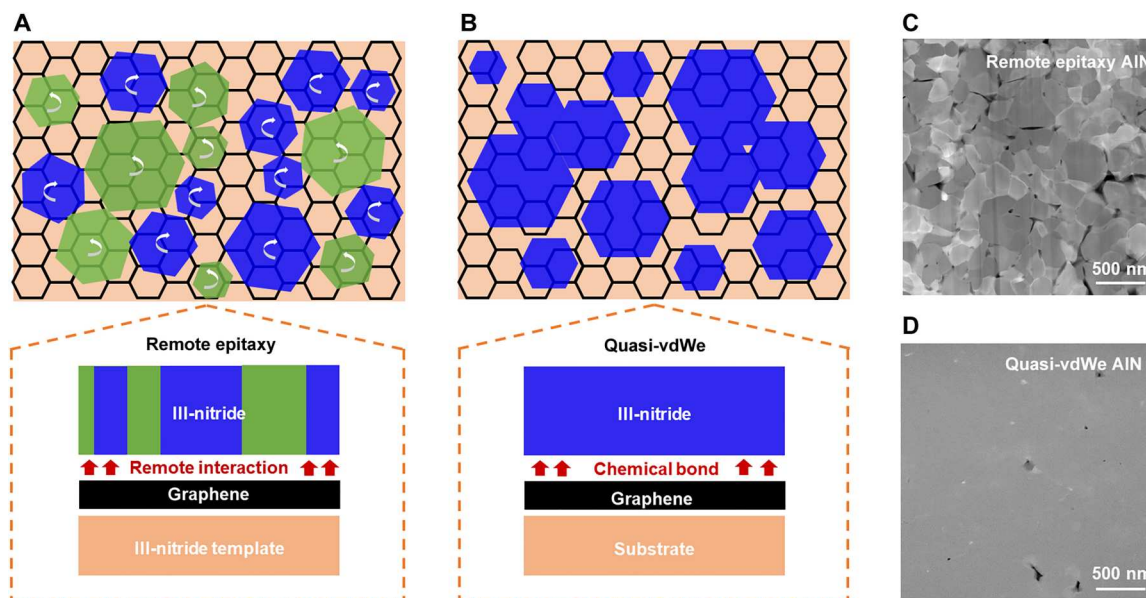


Fig. 5. Schematic illustration of III-nitride films grown on wet-transferred graphene. (A) Remote epitaxy of III-nitrides on Gr/III-nitride templates. In this case, the remote interaction is not sufficient to constrain III-nitride nuclei to inherit the in-plane orientation of the polar III-nitride template, resulting in the formation of randomly twisted nuclei. Here, nuclei with clockwise rotation are labeled blue and those with counter clockwise rotation are labeled green. As growth progresses, these misoriented nuclei expand to form twisted grains, eventually forming a polycrystalline film. (B) Quasi-vdWe of III-nitrides on single-crystal Gr. The substrate can be, for example, a single-crystal AlN template or a polycrystalline Mo. In this case, unsaturated dangling bonds on the Gr surface act as nucleation sites, triggering highly oriented III-nitride nucleation. These nucleation islands coalesce precisely and eventually form a single-crystal III-nitride film. (C) Planar HAADF-STEM image of AlN grown on a wet-transferred one-ML Gr/AlN(0001) template by remote epitaxy. Because of the substantial difference in orientation, the twisted remote epitaxial grains cannot coalesce to form a continuous AlN film. Besides, the surface fluctuation of Gr may cause the upper AlN to have a small tilt angle (less than 1°) with respect to the bottom AlN template. Off-axis grains generate a different contrast than on-axis grains because of channeling effect. (D) Planar HAADF-STEM image of AlN film grown on a wet-transferred three-ML Gr/AlN(0001) template by quasi-vdWe. The aligned grains nearly coalesce to form a single-crystal film. Here, the atomic N irradiation time of three-ML Gr is 3 min. The thickness of AlN films (C and D) is ~ 500 nm, and the planar STEM position is ~ 200 nm from the interface.

case, the single-crystal III-nitride film grows on wet-transferred graphene and is no longer strictly constrained by the underlying substrate (figs. S15 to S18). The lattice polarity of single-crystal films can be manipulated by adjusting the interfacial atomic configuration, i.e., interfacial covalent bond form (19, 28, 29, 51). Because of the stronger effect of chemical bonds on the superstructure than the effect of remote interactions (nonchemical bond form), quasi-vdWe is more inclusive in the choice of graphene and substrate materials, making it easier to achieve high-quality transferable III-nitride films (figs. S14D and S16, E and F). It should be noted that when graphene is not thick enough, the growth mode of epilayers may not be pure quasi-vdWe, i.e., thru-hole epitaxy may happen as well. Fortunately, through modulating the orientation of the quasi-van der Waals epitaxial grains, we are able to control them to exhibit almost the same orientation as those thru-hole epitaxial grains, resulting in a single-crystal film. Thus, it can be concluded that quasi-vdWe is the preferred route for the growth of single-crystal III-nitride films on wet-transferred graphene.

In conclusion, we report remote epitaxy and quasi-vdWe of polar III-nitride films on wet-transferred graphene and illustrate that quasi-vdWe is the preferred strategy of growth for single-crystal films. Here, using highly polar AlN as an example, it is found that the remote interaction from the graphene/AlN template can constrain the out-of-plane lattice inversion of nuclei but not their twist, resulting in a polycrystalline AlN film. This indicates that remote epitaxy is a promising method for realizing transferable

III-nitride thin films, but there is a certain technical threshold. Fine manipulation of III-nitride growth kinetics and higher-quality graphene interlayers is necessary to achieve single-crystal films. In the case of quasi-vdWe, III-nitride is mainly coupled with graphene through interface covalent bonds and establishes an epitaxial relationship, resulting in a single-crystal film. The interfacial chemical bond plays an important role in the formation of the epitaxial registry between the III-nitride film and graphene. Thence, the quasi-vdWe has a better tolerance for the quality of transferred graphene and the selection of the underlying substrate. The results of this work settle the debate about the preferred epitaxy and will promote the development of advanced III-nitride semiconductor devices on wet-transferred two-dimensional materials such as graphene.

MATERIALS AND METHODS

Computational model

Ab initio calculations were used in the density functional theory (DFT) framework with projector-augmented wave basis sets using the Vienna Ab Initio Simulation Package. The Perdew-Burke-Ernzerhof exchange-correlation functional was used with a 400 eV kinetic energy cutoff and a Γ -only k-point grid. The DFT-D3 method with Becke-Jonson damping was used to explicitly include the van der Waals interaction. We created a supercell consisting of $3 \times 3 \times 3$ wurtzite AlN to simulate the AlN bulk, $3 \times 3 \times 1$

AlN and $4 \times 4 \times 1$ graphene to simulate the epitaxial AlN and the graphene ML. The configuration (i.e., supercell) is periodic with no boundaries in the (0001) plane, and a 20 \AA thick vacuum gap was adopted to avoid the interaction between periodic images in the [0001] direction. Here, to explore the effect of remote interactions of graphene ML/AlN bulk on the atomic structure of epitaxial AlN, the binding energies (E_b) of the $3 \times 3 \times 1$ AlN in eight configurations (Fig. 1A) were calculated. The binding energy is defined by the overall epitaxial structure in each configuration. The more negative E_b is, the more stable the structure is. Four preferred configurations (I, II, V, and VI; Fig. 1A) and corresponding atomic structures of epitaxial AlN were found. Next, the contribution of the number of graphene layers to the remote interaction was demonstrated by increasing the graphene thickness from one to five MLs (Fig. 1D). We selected a one-ML graphene/AlN bulk case, which can provide the strongest remote interaction, as an example, to explore the influence of remote interaction on the in-plane orientation of AlN nuclei. Here, epitaxial AlN in configurations I, II, V, and VI (Fig. 1A) was simplified to a cluster structure (R-AlN) consisting of six Al atoms and six N atoms to simulate the AlN nuclei and formed four configurations (R-I, R-II, R-V, and R-VI; Fig. 1E). On the basis of the same periodic boundary conditions, the binding energies of entire R-AlN at different rotation angles from 0° to 60° along the [0001] axis across its center were calculated (Fig. 1, F and G). Other details and more are shown in figs. S1 to S5. Computational resources were provided by the Supercomputer Center of Peking University.

Fabrication of single-crystal AlN templates

For the AlN(0001) templates, Al-polar AlN films were grown on 2-inch Al_2O_3 (0001) substrates by MOCVD. The thickness of the Al-polar AlN layer was about $1.5 \mu\text{m}$. The detailed procedure is described in our previous reports (36). For the AlN(000 $\bar{1}$) templates, AlN films with N lattice polarity were grown on 2-inch 4H-SiC(000 $\bar{1}$) substrates by plasma-assisted MBE (SVT Associates MBE). The thickness of the N-polar AlN layer was about 120 nm (fig. S8). During N-polar AlN growth, the N_2 flow rate was 1.0 standard cubic centimeters per minute (sccm), the plasma power was 480 W, and the beam equivalent pressure of the Al atom beam was 4.0×10^{-7} mbar.

Wet-transfer of graphene

The growth of ultraflat single-crystal graphene ML on Cu(111)/ Al_2O_3 (0001) was performed as described in previous reports (4–6). The graphene ML was transferred to the AlN template surface by a poly(methyl methacrylate) (PMMA)-mediated transfer process. First, a layer of PMMA was spin-coated on graphene/Cu/ Al_2O_3 , and was then cured at 130°C to form a supporting film. The PMMA/graphene film was then detached from the growth substrate by etching the Cu film (500 nm in thickness) in an aqueous solution of $(\text{NH}_4)_2\text{S}_2\text{O}_8$ (1 mol/l). After being cleaned with deionized water, the PMMA/graphene film was attached to the target substrate, dried at room temperature, and baked at 180°C for 3 hours. Then, the PMMA layer was removed by hot acetone, leaving one-ML graphene on the target substrate. The two- to three-ML graphene samples were obtained by a layer-by-layer transfer method (52). The transferred graphene/AlN templates were annealed under an ambient of hydrogen (100 sccm) and argon (300 sccm) at 350°C

for 3 hours to remove organic and oxide residues. The size of the graphene was about $10 \times 10 \text{ mm}^2$ or $20 \times 20 \text{ mm}^2$.

Remote epitaxy of III-nitrides

Remote epitaxy of III-nitrides was performed by MOCVD (AIXTRON 19×2 inches). The AlN growth was performed at 1000°C with hydrogen as the carrier gas, and the flow rates of trimethylaluminum and ammonia were $157 \mu\text{mol}/\text{min}$ and 1000 sccm, respectively. On the other hand, for GaN growth performed at 1000°C , the flow rates of trimethylgallium and ammonia were $673 \mu\text{mol}/\text{min}$ and 18000 sccm, respectively.

Quasi-vdWe of III-nitrides

Quasi-vdWe of III-nitride films were performed by MOCVD (AIXTRON 19×2 inches) or MBE (PREVAC MBE). Transferred graphene was activated by a N-plasma source at 800°C in the MBE chamber (fig. S15A). Atomic N irradiation was applied for 1, 2, and 3 min with an N_2 flow rate of 0.8 sccm and a forward radio frequency plasma power of 350 W for one-ML, two-ML, and three-ML graphene, respectively, to form unsaturated C–N dangling bonds on the surface. The MOCVD growth parameters of III-nitrides on activated graphene were the same as those of the remote-epitaxial case. The MBE growth temperature was 800°C , the N_2 flow rate was 0.8 sccm, the plasma power was 350 W, and the beam equivalent pressures of Al and Ga atom beams were 3.5×10^{-7} mbar and 8.0×10^{-7} mbar, respectively.

Characterization

The surface morphologies of graphene and III-nitrides were measured by atomic force microscopy in ScanAsyst mode (Bruker Dimension ICON). The structural quality of graphene was characterized by Raman scattering spectroscopy (Horiba LabRAM HR Evolution Raman system; 532 nm laser excitation with a laser spot diameter of $1 \mu\text{m}$). The surface morphology of III-nitride films was also measured by high-resolution SEM (Thermo Fisher Scientific, Helios G4 UX). Bruker CrystAlign EBSD and in situ SEM (not high-resolution mode) were used to determine the crystal orientation of the film. Before SEM and EBSD measurements, a conductive carbon film with a thickness of 10 nm was deposited on the insulated AlN at room temperature. Spherical aberration-corrected STEM (FEI Titan Cubed Themis G2 60-300) was used to determine the atomic arrangement of the III-nitride/graphene interface. The STEM samples were prepared by a focused ion beam system (Thermo Fisher Scientific, Helios G4 UX). For planar STEM measurements, 60 nm thick lamellas were extracted from the near intermediate region of the 500 nm thick AlN film. In planar HAADF-STEM images (Fig. 5C), the contrast generated by off-axis grains is different from that generated by on-axis grains due to channeling effects (53). XRD measurements were performed by an X'Pert3 MRD system using a Cu K α 1 x-ray source. Here, for quasi-van der Waals epitaxial III-nitride films (Fig. 4 and figs. S16 to S18) and GaN films obtained by ELOG (fig. S14), the sample needs to be cut before XRD testing to remove the regions without graphene. To eliminate the interference of other growth paths as much as possible, the stripped remote epitaxial films are tested by XRD (fig. S13).

Supplementary Materials

This PDF file includes:

Supplementary Text

Figs. S1 to S18

References

REFERENCES AND NOTES

- X. Z. Xu, Z. Zhang, L. Qiu, J. Zhuang, L. Zhang, H. Wang, C. Liao, H. Song, R. Qiao, P. Gao, Z. Hu, L. Liao, Z. Liao, D. Yu, E. Wang, F. Ding, H. Peng, K. Liu, Ultrafast growth of single-crystal graphene assisted by a continuous oxygen supply. *Nat. Nanotechnol.* **11**, 930–935 (2016).
- C. Liu, Z. Li, R. Qiao, Q. Wang, Z. Zhang, F. Liu, Z. Zhou, N. Shang, H. Fang, M. Wang, Z. Liu, Z. Feng, Y. Cheng, H. Wu, D. Gong, S. Liu, Z. Zhang, D. Zou, Y. Fu, J. He, H. Hong, M. Wu, P. Gao, P. H. Tan, X. Wang, D. Yu, E. Wang, Z. J. Wang, K. Liu, Designed growth of large bilayer graphene with arbitrary twist angles. *Nat. Mater.* **21**, 1263–1268 (2022).
- T. R. Wu, X. Zhang, Q. Yuan, J. Xue, G. Lu, Z. Liu, H. Wang, H. Wang, F. Ding, Q. Yu, X. Xie, M. Jiang, Fast growth of inch-sized single-crystalline graphene from a controlled single nucleus on Cu–Ni alloys. *Nat. Mater.* **15**, 43–47 (2016).
- B. Deng, Z. Pang, S. Chen, X. Li, C. Meng, J. Li, M. Liu, J. Wu, Y. Qi, W. Dang, H. Yang, Y. Zhang, J. Zhang, N. Kang, H. Xu, Q. Fu, X. Qiu, P. Gao, Y. Wei, Z. Liu, H. Peng, Wrinkle-free single-crystal graphene wafer grown on strain-engineered substrates. *ACS Nano* **11**, 12337–12345 (2017).
- L. Lin, J. Zhang, H. Su, J. Li, L. Sun, Z. Wang, F. Xu, C. Liu, S. Lopatin, Y. Zhu, K. Jia, S. Chen, D. Rui, J. Sun, R. Xue, P. Gao, N. Kang, Y. Han, H. Q. Xu, Y. Cao, K. S. Novoselov, Z. Tian, B. Ren, H. Peng, Z. Liu, Towards super-clean graphene. *Nat. Commun.* **10**, 1912 (2019).
- X. Gao, L. Zheng, F. Luo, J. Qian, J. Wang, M. Yan, W. Wang, Q. Wu, J. Tang, Y. Cao, C. Tan, J. Tang, M. Zhu, Y. Wang, Y. Li, L. Sun, G. Gao, J. Yin, L. Lin, Z. Liu, S. Qin, H. Peng, Integrated wafer-scale ultra-flat graphene by gradient surface energy modulation. *Nat. Commun.* **13**, 5410 (2022).
- Y. Zhao, Y. Song, Z. Hu, W. Wang, Z. Chang, Y. Zhang, Q. Lu, H. Wu, J. Liao, W. Zou, X. Gao, K. Jia, L. Zhuo, J. Hu, Q. Xie, R. Zhang, X. Wang, L. Sun, F. Li, L. Zheng, M. Wang, J. Yang, B. Mao, T. Fang, F. Wang, H. Zhong, W. Liu, R. Yan, J. Yin, Y. Zhang, Y. Wei, H. Peng, L. Lin, Z. Liu, Large-area transfer of two-dimensional materials free of cracks, contamination and wrinkles via controllable conformal contact. *Nat. Commun.* **13**, 4409 (2022).
- Z. Chen, Z. Liu, T. Wei, S. Yang, Z. Dou, Y. Wang, H. Ci, H. Chang, Y. Qi, J. Yan, J. Wang, Y. Zhang, P. Gao, J. Li, Z. Liu, Improved epitaxy of AlN film for deep-ultraviolet light-emitting diodes enabled by graphene. *Adv. Mater.* **31**, e1807345 (2019).
- K. Chung, C. H. Lee, G. C. Yi, Transferable GaN layers grown on ZnO-coated graphene layers for optoelectronic devices. *Science* **330**, 655–657 (2010).
- D. S. Liu, L. Hu, X. Yang, Z. Zhang, H. Yu, F. Zheng, Y. Feng, J. Wei, Z. Cai, Z. Chen, C. Ma, F. Xu, X. Wang, W. Ge, K. Liu, B. Huang, B. Shen, Polarization-driven-orientation selective growth of single-crystalline III-nitride semiconductors on arbitrary substrates. *Adv. Funct. Mater.* **32**, 2113211 (2022).
- J. Jeong, Q. Wang, J. Cha, D. K. Jin, D. H. Shin, S. Kwon, B. K. Kang, J. H. Jang, W. S. Yang, Y. S. Choi, J. Yoo, J. K. Kim, C.-H. Lee, S. W. Lee, A. Zakhidov, S. Hong, M. J. Kim, Y. J. Hong, Remote heteroepitaxy of GaN microrod heterostructures for deformable light-emitting diodes and wafer recycle. *Sci. Adv.* **6**, eaaz5180 (2020).
- J. Jeong, D. K. Jin, J. Choi, J. Jang, B. K. Kang, Q. Wang, W. I. Park, M. S. Jeong, B. S. Bae, W. S. Yang, M. J. Kim, Y. J. Hong, Transferable, flexible white light-emitting diodes of GaN p-n junction microcrystals fabricated by remote epitaxy. *Nano Energy* **86**, 106075 (2021).
- S. Nakamura, The roles of structural imperfections in InGaN-Based blue light-emitting diodes and laser diodes. *Science* **281**, 956–961 (1998).
- H. Amano, Nobel Lecture: Growth of GaN on sapphire via low-temperature deposited buffer layer and realization of p-type GaN by Mg doping followed by low-energy electron beam irradiation. *Rev. Mod. Phys.* **87**, 1133–1138 (2015).
- J. Kim, C. Bayram, H. Park, C. W. Cheng, C. Dimitrakopoulos, J. A. Ott, K. B. Reuter, S. W. Bedell, D. K. Sadana, Principle of direct van der Waals epitaxy of single-crystalline films on epitaxial graphene. *Nat. Commun.* **5**, 4836 (2014).
- F. Ren, B. Liu, Z. Chen, Y. Yin, J. Sun, S. Zhang, B. Jiang, B. Liu, Z. Liu, J. Wang, M. Liang, G. Yuan, J. Yan, T. Wei, X. Yi, J. Wang, Y. Zhang, J. Li, P. Gao, Z. Liu, Z. Liu, Van der Waals epitaxy of nearly single-crystalline nitride films on amorphous graphene-glass wafer. *Sci. Adv.* **7**, eabf5011 (2021).
- Y. Kim, S. S. Cruz, K. Lee, B. O. Alawode, C. Choi, Y. Song, J. M. Johnson, C. Heidelberg, W. Kong, S. Choi, K. Qiao, I. Almansouri, E. A. Fitzgerald, J. Kong, A. M. Kolpak, J. Hwang, J. Kim, Remote epitaxy through graphene enables two-dimensional material-based layer transfer. *Nature* **544**, 340–343 (2017).
- H. Kim, K. Lu, Y. Liu, H. S. Kum, K. S. Kim, K. Qiao, S. H. Bae, S. Lee, Y. J. Ji, K. H. Kim, H. Paik, S. Xie, H. Shin, C. Choi, J. H. Lee, C. Dong, J. A. Robinson, J. H. Lee, J. H. Ahn, G. Y. Yeom, D. G. Schlom, J. Kim, Impact of 2D–3D heterointerface on remote epitaxial interaction through graphene. *ACS Nano* **15**, 10587–10596 (2021).
- F. Liu, T. Wang, Z. Zhang, T. Shen, X. Rong, B. Sheng, L. Yang, D. Li, J. Wei, S. Sheng, X. Li, Z. Chen, R. Tao, Y. Yuan, X. Yang, F. Xu, J. Zhang, K. Liu, X.-Z. Li, B. Shen, X. Wang, Lattice polarity manipulation of quasi-vdW epitaxial GaN films on graphene through interface atomic configuration. *Adv. Mater.* **34**, 2106814 (2022).
- J. Yu, L. Wang, Z. Hao, Y. Luo, C. Sun, J. Wang, Y. Han, B. Xiong, H. Li, Van der Waals epitaxy of III-nitride semiconductors based on 2D materials for flexible applications. *Adv. Mater.* **32**, e1903407 (2020).
- A. Koma, Van der Waals epitaxy—A new epitaxial growth method for a highly lattice-mismatched system. *Thin Solid Films* **216**, 72–76 (1992).
- Z. H. Zhang, X. N. Yang, K. H. Liu, R. M. Wang, Epitaxy of 2D materials toward single-crystals. *Adv. Sci.* **9**, 2105201 (2022).
- Y. Liu, Y. Huang, X. F. Duan, Van der Waals integration before and beyond two-dimensional materials. *Nature* **567**, 323–333 (2019).
- K. Qiao, Y. Liu, C. Kim, R. J. Molnar, T. Osadchy, W. Li, X. Sun, H. Li, R. L. Myers-Ward, D. Lee, S. Subramanian, H. Kim, K. Lu, J. A. Robinson, W. Kong, J. Kim, Graphene buffer layer on SiC as a release layer for high-quality freestanding semiconductor membranes. *Nano Lett.* **21**, 4013–4020 (2021).
- W. Kong, H. Li, K. Qiao, Y. Kim, K. Lee, Y. Nie, D. Lee, T. Osadchy, R. J. Molnar, D. K. Gaskill, R. L. Myers-Ward, K. M. Daniels, Y. Zhang, S. Sundram, Y. Yu, S. H. Bae, S. Rajan, Y. Shao-Horn, K. Cho, A. Ougazzaden, J. C. Grossman, J. Kim, Polarity governs atomic interaction through two-dimensional materials. *Nat. Mater.* **17**, 999–1004 (2018).
- Y. Chen, H. Zang, K. Jiang, J. Ben, S. Zhang, Z. Shi, Y. Jia, W. Lü, X. Sun, D. Li, Improved nucleation of AlN on in situ nitrogen doped graphene for GaN quasi-van der Waals epitaxy. *Appl. Phys. Lett.* **117**, 051601 (2020).
- Y. Song, Y. Gao, X. Liu, J. Ma, B. Chen, Q. Xie, X. Gao, L. Zheng, Y. Zhang, Q. Ding, K. Jia, L. Sun, W. Wang, Z. Liu, B. Liu, P. Gao, H. Peng, T. Wei, L. Lin, Z. Liu, Transfer-enabled fabrication of graphene wrinkle arrays for epitaxial growth of AlN films. *Adv. Mater.* **34**, e2105851 (2022).
- H. Chang, Z. Chen, B. Liu, S. Yang, D. Liang, Z. Dou, Y. Zhang, J. Yan, Z. Liu, Z. Zhang, J. Wang, J. Li, Z. Liu, P. Gao, T. Wei, Quasi-2D growth of aluminum nitride film on graphene for boosting deep ultraviolet light-emitting diodes. *Adv. Sci.* **7**, 2105851 (2020).
- F. Liu, Z. Zhang, X. Rong, Y. Yu, T. Wang, B. Sheng, J. Wei, S. Zhou, X. Yang, F. Xu, Z. Qin, Y. Zhang, K. Liu, B. Shen, X. Wang, Graphene-assisted epitaxy of nitrogen lattice polarity gan films on non-polar sapphire substrates for green light emitting diodes. *Adv. Funct. Mater.* **30**, 2001283 (2020).
- V. Kumaresan, L. Largeau, A. Madouri, F. Glas, H. Zhang, F. Oehler, A. Cavanna, A. Babichev, L. Travers, N. Gogneau, M. Tchernycheva, J. C. Harmand, Epitaxy of GaN nanowires on graphene. *Nano Lett.* **16**, 4895–4902 (2016).
- A. Filippetti, V. Fiorentini, G. Cappellini, A. Bosin, Anomalous relaxations and chemical trends at III-V semiconductor nitride nonpolar surfaces. *Phys. Rev. B* **59**, 8026–8031 (1999).
- E. K. Yu, D. A. Stewart, S. Tiwari, Ab initio study of polarizability and induced charge densities in multilayer graphene films. *Phys. Rev. B* **77**, 195406 (2008).
- L. Pietronero, S. Strassler, H. R. Zeller, M. J. Rice, Charge distribution in c direction in lamellar graphite acceptor intercalation compounds. *Phys. Rev. Lett.* **41**, 763–767 (1978).
- K. S. Novoselov, A. K. Geim, S. V. Morozov, D. Jiang, Y. Zhang, S. V. Dubonos, I. V. Grigorieva, A. A. Firsov, Electric field effect in atomically thin carbon films. *Science* **306**, 666–669 (2004).
- J. M. Luttinger, L. Tisza, Theory of dipole interaction in crystals. *Phys. Rev.* **70**, 954–964 (1946).
- S. Liu, Y. Yuan, L. Huang, J. Zhang, T. Wang, T. Li, J. Kang, W. Luo, Z. Chen, X. Sun, X. Wang, Drive high power UVC-LED wafer into low-cost 4-inch era: Effect of strain modulation. *Adv. Funct. Mater.* **32**, 2112111 (2022).
- Y. Qi, Y. Wang, Z. Pang, Z. Dou, T. Wei, P. Gao, S. Zhang, X. Xu, Z. Chang, B. Deng, S. Chen, Z. Chen, H. Ci, R. Wang, F. Zhao, J. Yan, X. Yi, K. Liu, H. Peng, Z. Liu, L. Tong, J. Zhang, Y. Wei, J. Li, Z. Liu, Fast growth of strain-free AlN on graphene-buffered sapphire. *J. Am. Chem. Soc.* **140**, 11935–11941 (2018).
- K. Kim, S. Coh, L. Z. Tan, W. Regan, J. M. Yuk, E. Chatterjee, M. F. Crommie, M. L. Cohen, S. G. Louie, A. Zettl, Raman spectroscopy study of rotated double-layer graphene: Mis-orientation-angle dependence of electronic structure. *Phys. Rev. Lett.* **108**, 246103 (2012).
- J. H. Park, J. Y. Lee, M. D. Park, J. H. Min, J. S. Lee, X. Yang, S. Kang, S. J. Kim, W. L. Jeong, H. Amano, D. S. Lee, Influence of temperature-dependent substrate decomposition on graphene for separable gan growth. *Adv. Mater. Interfaces* **6**, 1900821 (2019).
- J. H. Park, X. Yang, J. Y. Lee, M. D. Park, S. Y. Bae, M. Pristovsek, H. Amano, D. S. Lee, The stability of graphene and boron nitride for III-nitride epitaxy and post-growth exfoliation. *Chem. Sci.* **12**, 7713–7719 (2021).
- G. Fasol, Longer life for the blue laser. *Science* **278**, 1902–1903 (1997).

42. X. Han, J. Yu, Z. Li, X. Wang, Z. Hao, Y. Luo, C. Sun, Y. Han, B. Xiong, J. Wang, H. Li, Y. Zhang, B. Duan, J. Ning, H. Wu, L. Wang, Remote epitaxy and exfoliation of GaN via graphene. *ACS Appl. Electron Mater.* **4**, 5326–5332 (2022).
43. H. Kim, C. S. Chang, S. Lee, J. Jiang, J. Jeong, M. Park, Y. Meng, J. Ji, Y. Kwon, X. Sun, W. Kong, H. S. Kum, S. H. Bae, K. Lee, Y. J. Hong, J. Shi, J. Kim, Remote epitaxy. *Nat. Rev. Methods Primers* **2**, 40 (2022).
44. J. Kim, G. C. Yi, A. Ougazzaden, J. Shi, Novel epitaxy of functional materials. *J. Appl. Phys.* **132**, 060401 (2022).
45. J. Shin, H. Kim, S. Sundaram, J. Jeong, B. I. Park, C. S. Chang, J. Choi, T. Kim, M. Saravanapavanantham, K. Lu, S. Kim, J. M. Suh, K. S. Kim, M. K. Song, Y. Liu, K. Qiao, J. H. Kim, Y. Kim, J. H. Kang, J. Kim, D. Lee, J. Lee, J. S. Kim, H. E. Lee, H. Yeon, H. S. Kum, S. H. Bae, V. Bulovic, K. J. Yu, K. Lee, K. Chung, Y. J. Hong, A. Ougazzaden, J. Kim, Vertical full-colour micro-LEDs via 2D materials-based layer transfer. *Nature* **614**, 81–87 (2023).
46. J. H. Ji, H.-M. Kwak, J. Yu, S. Park, J.-H. Park, H. Kim, S. Kim, S. Kim, D.-S. Lee, H. S. Kum, Understanding the 2D-material and substrate interaction during epitaxial growth towards successful remote epitaxy: A review. *Nano Converg.* **10**, 19 (2023).
47. M. Bah, D. Valente, M. Lesecq, N. Defrance, M. Garcia Barros, J. C. de Jaeger, E. Frayssinet, R. Comyn, T. H. Ngo, D. Alquier, Y. Cordier, Electrical activity at the AlN/Si Interface: Identifying the main origin of propagation losses in GaN-on-Si devices at microwave frequencies. *Sci. Rep.* **10**, 14166 (2020).
48. T. Novak, P. Kostelnik, M. Koněný, J. Čechal, M. Kolíbal, T. Šíkola, Temperature effect on Al predeposition and AlN nucleation affecting the buffer layer performance for the GaN-on-Si based high-voltage devices. *Jpn. J. Appl. Phys.* **58**, SC1018 (2019).
49. D. Jang, C. Ahn, Y. Lee, S. Lee, H. Lee, D. Kim, Y. Kim, J. Y. Park, Y. K. Kwon, J. Choi, C. Kim, Thru-hole epitaxy: A highway for controllable and transferable epitaxial growth. *Adv. Mater. Interfaces* **10**, 2201406 (2023).
50. S. Manzo, P. J. Strohbeen, Z. H. Lim, V. Saraswat, D. du, S. Xu, N. Pokharel, L. J. Mawst, M. S. Arnold, J. K. Kawasaki, Pinhole-seeded lateral epitaxy and exfoliation of GaSb films on graphene-terminated surfaces. *Nat. Commun.* **13**, 4014 (2022).
51. F. Liu, Y. Yu, Y. Zhang, X. Rong, T. Wang, X. Zheng, B. Sheng, L. Yang, J. Wei, X. Wang, X. Li, X. Yang, F. Xu, Z. Qin, Z. Zhang, B. Shen, X. Wang, Hexagonal BN-assisted epitaxy of strain released GaN films for true green light-emitting diodes. *Adv. Sci.* **7**, 2000917 (2020).
52. Y. Wang, S. W. Tong, X. F. Xu, B. Ozyilmaz, K. P. Loh, Interface engineering of layer-by-layer stacked graphene anodes for high-performance organic solar cells. *Adv. Mater.* **23**, 1514–1518 (2011).
53. D. C. Joy, D. E. Newbury, D. L. Davidson, Electron channeling patterns in the scanning electron-microscope. *J. Appl. Phys.* **53**, R81–R122 (1982).
54. M. Wang, M. Huang, D. Luo, Y. Li, M. Choe, W. K. Seong, M. Kim, S. Jin, M. Wang, S. Chatterjee, Y. Kwon, Z. Lee, R. S. Ruoff, Single-crystal, large-area, fold-free monolayer graphene. *Nature* **596**, 519–524 (2021).
55. Y. P. Qu, Y. Xu, B. Cao, Y. Wang, J. Wang, L. Shi, K. Xu, Long-range orbital hybridization in remote epitaxy: The nucleation mechanism of GaN on different substrates via single-layer graphene. *ACS Appl. Mater. Interfaces* **14**, 2263–2274 (2022).
56. A. V. Kretinin, Y. Cao, J. S. Tu, G. L. Yu, R. Jalil, K. S. Novoselov, S. J. Haigh, A. Gholinia, A. Mishchenko, M. Lozada, T. Georgiou, C. R. Woods, F. Withers, P. Blake, G. Eda, A. Wirsig, C. Hucho, K. Watanabe, T. Taniguchi, A. K. Geim, R. V. Gorbachev, Electronic properties of graphene encapsulated with different two-dimensional atomic crystals. *Nano Lett.* **14**, 3270–3276 (2014).
57. L. G. Cancado, A. Jorio, E. H. Martins Ferreira, F. Stavale, C. A. Achete, R. B. Capaz, M. V. O. Moutinho, A. Lombardo, T. S. Kulmala, A. C. Ferrari, Quantifying defects in graphene via Raman spectroscopy at different excitation energies. *Nano Lett.* **11**, 3190–3196 (2011).
58. O. Ledyev, M. Pandikunta, S. Nikishin, N-polar AlN thin layers grown on Si(111) by plasma-assisted MBE. *Jpn. J. Appl. Phys.* **53**, 050306 (2014).
59. A. Kovács, M. Duchamp, R. E. Dunin-Borkowski, R. Yakimova, P. L. Neumann, H. Behmenburg, B. Foltynski, C. Giesen, M. Heuken, B. Pécz, Graphoepitaxy of high-quality GaN layers on graphene/6H-SiC. *Adv. Mater. Interfaces* **2**, 1400230 (2015).
60. Q. Chen, K. Yang, B. Shi, X. Yi, J. Wang, J. Li, Z. Liu, Principles for 2D-material-assisted nitrides epitaxial growth. *Adv. Mater.* **35**, e2211075 (2023).
61. Y. Yin, B. Liu, Q. Chen, Z. Chen, F. Ren, S. Zhang, Z. Liu, R. Wang, M. Liang, J. Yan, J. Sun, X. Yi, T. Wei, J. Wang, J. Li, Z. Liu, P. Gao, Z. Liu, Continuous single-crystalline GaN film grown on WS₂-Glass wafer. *Small* **18**, 2202529 (2022).

Acknowledgments

Funding: X.W. acknowledges the National Key R&D Program of China (no. 2021YFA0716400), the National Natural Science Foundation of China (no. 62227817), and the Beijing Outstanding Young Scientist Program (no. BJJWZYJH0120191000103). H.P. acknowledges the National Natural Science Foundation of China (nos. 52021006 and T2188101). X.-Z.L. acknowledges the National Natural Science Foundation of China (nos. 11934003 and 12234001). F.L. acknowledges the National Key R&D Program of China (no. 2022YFB3608100), the National Natural Science Foundation of China (no. 62104010), and the China National Postdoctoral Program for Innovative Talents (no. BX2021007). **Author contributions:** X.W. conceived the project. H.Y., F.L., and X.-Z.L. designed theoretical models and performed DFT calculations. X.G., Z.Z., J.T., K.L., and H.P. performed the growth and transfer of graphene. F.L., B. Sheng, Y.Y., Z.C., and B. Shen conducted the growth of AlN templates. F.L., T.W., Z.H., X.G., and Y.G. performed the growth and characterization of III-nitride films. All authors contributed to the discussion of the results. **Competing interests:** The authors declare that they have no competing interests. **Data and materials availability:** All data needed to evaluate the conclusions in the paper are present in the paper and/or the Supplementary Materials.

Submitted 17 November 2022

Accepted 5 July 2023

Published 2 August 2023

10.1126/sciadv.adf8484